Langmuir

Article

pubs.acs.org/Langmuir

Stability of $C_{12}E_j$ Bilayers Probed with Adhesive Droplets

Ksenia Astafyeva,[†] Wladimir Urbach,[†,‡] Nabil Garroum,[†] Nicolas Taulier,[§] and Abdou R. Thiam*[,†]

[†]Laboratoire de Physique Statistique, Ecole Normale Supérieure, Sorbonne Universités, UPMC Université, and Université Paris Diderot, CNRS, 24 rue Lhomond, F-75005 Paris, France

[‡]Université René Descartes, Paris, France

[§]Sorbonne Universités, UPMC Univ. Paris 06, CNRS, Laboratoire d'Imagerie Biomédicale, INSERM, F-75006 Paris, France

Supporting Information

ABSTRACT: The stability of model surfactant bilayers from the poly(ethylene glycol) mono-*n*-dodecyl ether ($C_{12}E_j$) family was probed. The surfactant bilayers were formed by the adhesion of emulsion droplets. We generated $C_{12}E_j$ bilayers by forming water-in-oil (w/o) emulsions with saline water droplets, covered by the surfactant, in a silicone and octane oil mixture. Using microfluidics, we studied the stability of those bilayers. $C_{12}E_1$ allowed only short-lived bilayers whereas $C_{12}E_2$ bilayers were stable over a wide range of oil mixtures. At high $C_{12}E_2$ concentration, a two-phase region was displayed in the phase diagram: bilayers formed by the adhesion of two water droplets and Janus-like particles consisting of adhering aqueous and amphiphilic droplets. $C_{12}E_8$ and $C_{12}E_{25}$ did not mediate bilayer formation and caused phase inversion leading to o/w emulsion. With intermediate $C_{12}E_4$ and $C_{12}E_5$ surfactants, both w/o and o/w emulsions were unstable. We provided the titration of the $C_{12}E_2$ bilayer with $C_{12}E_4$ and $C_{12}E_5$ to study and predict their stability behavior.

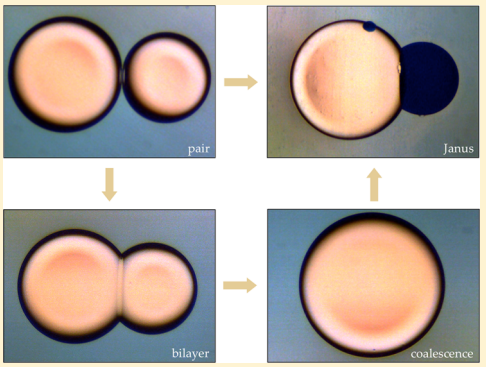

INTRODUCTION

Model bilayers are attractive for the reconstitution and characterization of the function of proteins.[1,2] Most of them are generated using phospholipids.[3−5] For intrinsic protein characterization, e.g., protein purification and crystallization,[6−8] artificial bilayers made of poly(oxyethylene) dodecyl ethers, (CH_3-$(CH_2)_{12}$−$(O$−CH_2−$CH_2)_j$−OH), $C_{12}E_j$, are often used.[9] They belong to the class of nonionic surfactants[10] forming synthetic bilayers,[11] which do not interfere with protein integration, as they do not introduce significant repulsion forces such as Lifshitz−van der Waals, hydrogen bonds, or electrostatic interactions,[12] as compared to other surfactants. They are easily synthesized with various lengths of the hydrophobic and hydrophilic segments that offers room for surfactant choice with regard to the protein environmental requirement. In addition, $C_{12}E_j$ bilayers exhibit high deformability, as their bending modulus is of the order of the thermal energy k_BT and hence displays interesting phase behavior. In aqueous buffer, they can form lamellar phase membranes (L_α), a stack of bilayers, or sponge phases (L_3)[13−15] resembling connected lamellar (or melted cubic) phases. The sponge phase of $C_{12}E_5$ was used to preserve the activity of transmembrane proteins,[16,17] and $C_{12}E_8$ allowed the solubilization and 2D crystallization of proteins.[18,19] Understanding the stability and structure of $C_{12}E_j$ bilayers is thus required.

Studying C_iE_j bilayers in bulk experiments requires heavy experimental approaches such as X-ray and a nontrivial description of membrane interaction. Working with isolated C_iE_j bilayers overcomes that and allows a better understanding of the biophysical properties of membranes. Droplet interface bilayers (DIBs)[20−22] offer such a solution. They are produced in inverse emulsions, i.e., water in oil (w/o) emulsions, by bringing together two aqueous droplets, covered by a surfactant monolayer, in the oil medium. Depending on the type of surfactant and oil, the droplets brought in contact may form a thermodynamically stable bilayer. Single bilayers are easily generated this way.[23]

DIBs were so far formed with naturally occurring lipids, e.g., phospholipids. The existing formulations did not allow the generation of $C_{12}E_j$-DIBs. This is because the thermodynamic mixture ($C_{12}E_j$ and oils) did not reach equilibrium with DIB formation. It was necessary to then find the right ingredients to generate DIBs for a specific $C_{12}E_j$ surfactant. Following the basic need to have a good and bad solvent mixture of the surfactants to make DIBs,[24,25] we generated the $C_{12}E_j$ bilayer by forming water-in-oil (w/o) emulsions with saline water droplets, covered by the surfactant, in a silicone and octane oil mixture. We studied the stability of the $C_{12}E_j$ bilayers. $C_{12}E_1$ allowed only short-lived bilayers, but $C_{12}E_2$ bilayers were stable over a wide range of oil mixtures. At high $C_{12}E_2$ concentration, a two-phase region was displayed in the phase diagram: bilayers formed by the adhesion of two water droplets and Janus droplets consisting of adhering aqueous and amphiphilic droplets. $C_{12}E_8$ and $C_{12}E_{25}$ did not mediate bilayer formation

Received: February 27, 2015
Revised: June 2, 2015
Published: June 2, 2015

DOI: 10.1021/acs.langmuir.5b00749
Langmuir 2015, 31, 6791−6796

and caused phase inversion leading to o/w emulsion. With intermediate $C_{12}E_4$ and $C_{12}E_5$ surfactants, both w/o and o/w emulsions were unstable. We provided the titration of the $C_{12}E_2$ bilayer with $C_{12}E_4$ and $C_{12}E_5$ to study and predict their stability behavior.

MATERIALS AND METHODS

Materials. Octane, sodium chloride, and chloro(trimethyl)silane, oil-soluble oil blue N, and water-soluble rhodamine B dyes were purchased from Sigma-Aldrich. Silicone oil and Rhodorsil 47 V 20 were from Rhodia. Poly(ethylene glycol) monododecyl ethers $C_{12}E_j$, with j = 1, 2, and 25 (95% purity), were purchased from TCI Chemicals, and surfactants with j = 4, 5, and 8 (98% purity) were purchased from Sigma-Aldrich. All chemicals were used as received. Water was purified with a Milli-Q system (Millipore).

For microfluidic devices, glass capillaries (Vitrocom) and PTFE tube coils (Idex) were assembled together with Loctite glue (Manutan).

For emulsions formulation in a microfluidic device, adhesive emulsions were formed using previous approaches.[25] However, the microfluidic glass capillary setup was used in our experiment not only for precisely controlling the droplet size but also, and mainly, for keeping the concentration of the different components constant. For $C_{12}E_j$ (j = 1, 2, 4, 5, 8, and 25) surfactants, the stabilization of the bilayer created by droplet adhesion was achieved using a subtle balance of oils, with each of them exhibiting either a stabilizing or destabilizing effect. Silicone oil was used as a poor solvent to favor hydrocarbon adhesion.[22,25] Octane naturally provides good solubility for hydrocarbons. Shorter hydrocarbon oils or dodecane as a good solvent allowed emulsion stability but not DIB formation. It should be emphasized, however, that the notion of good and bad solvents does not exclusively depend on the length on the hydrocarbon chain of the surfactant but potentially on its overall HLB. This is in part the reason that the choice of optimal solvents for DIB formation is not trivial. The presence of sodium chloride in water prevented surfactant precipitation. For a salt concentration of between 2.5 and 10%, the lifetime of the $C_{12}E_2$ DIBs was tremendously increased, more than 10 h. This range of salt concentration corresponds to a Debye length, λ_D, of less than 4.6 Å, which decreases the surface area of the surfactant hydrophilic head sufficiently to screen electrostatic interactions.

Emulsion droplets were formed in glass capillaries by flow focusing (Figure 1a). To prevent wetting of the aqueous phase on the glass, the capillaries were silanized with chloro(trimethyl)silane. The organic phase flowed through the corners of the square glass capillaries (1000 μL/h), and as soon as the different flows met at the mouthpiece, aqueous droplets were regularly formed in the oil phase (Figure 1b). The flow rate of the continuous phase was modulated (30−60 μL/h) to induce droplet size variation (200 ± 100 μm). As soon as many droplets were generated, we stopped the flow rates and observed that mainly droplets of different size were coming into contact to ultimately adhere and form a DIB. DIBs were defined as stable if their lifetime was more than 5 min, meaning that droplets did not coalesce. This time was sufficient to provide investigations of bilayer properties. Experiments were performed at room temperature; all volume fractions were determined with a precision of better than 1%.

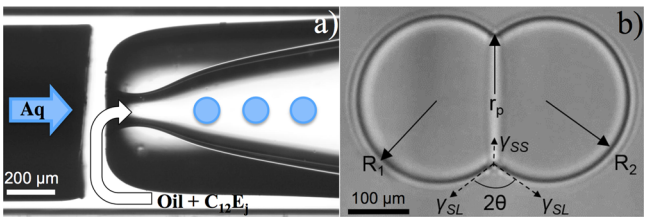

Figure 1. (a) Formation of w/o droplets by flow focusing in a glass capillary device. (b) Snapshot of two adhesive droplets along with the main parameters of the droplet pair: R_1 and R_2 are the adhesive droplets' radii, r_p is the radius of the bilayer, θ is the contact angle, γ_{SL} is the bulk interfacial tension of aqueous/oil phases interface in the presence of $C_{12}E_j$ surfactants, and γ_{SS} is the surface tension of the DIB.

Interfacial Tension Measurement and Adhesion Energy Calculation. The interfacial tension of pure oil mixture components and with excess $C_{12}E_1/C_{12}E_2$ surfactants was measured by the falling droplet method.[26] A droplet of the saline solution was flown vertically down into the oil phase from a constant slow pace. The drop falls once its volume reaches a maximal value reflected by the interfacial tension between two media. The interfacial tension, γ_{SL}, was deduced from the modified Tate's law,[26,27] $\gamma_{SL} = ((\Delta\rho g V)/(2\pi R\psi))$, where $\Delta\rho$ is the density difference of the liquids, g is gravity, V is the drop volume, R is the internal radius of a capillary, and $\psi = V/V_{ideal}$.

At equilibrium of adhesion, $2\gamma_{SS} = 2\gamma_{SL}(\cos\theta)$, where the contact angle θ is given by $2\theta = \sin^{-1}(r_p/R_1) + \sin^{-1}(r_p/R_2)$, r_p and $R_{1,2}$ are, respectively, the patch and droplet radii (Figure 1b), and γ_{SL} is the interfacial tension of the aqueous solution and silicone oil/octane interface saturated with surfactants. The adhesion energy, E, of the bilayer is derived from the Young−Dupré equation,[25] $E = 2\gamma_{SL}(1 - \cos\theta)$.

RESULTS AND DISCUSSION

Stability with Short-Head Surfactants and Phase Diagram of $C_{12}E_2$. $C_{12}E_1$ and $C_{12}E_2$ were stabilized w/o emulsion due to their low HLB[28] (5.3 for $C_{12}E_1$ and 7.7 for $C_{12}E_2$) and allowed the formation of DIBs between close droplets. However, $C_{12}E_1$ DIBs often coalesced in less than 5 min, regardless of the surfactant concentration. $C_{12}E_2$ emulsions were more stable (more than 1 day), which allowed us to study their stability phase diagram (Figure 2a). We identified three main regions. In region I, at low silicon oil content (SO) and/or $C_{12}E_2$ concentrations, w/o droplets directly coalesced when approaching each other or first formed a DIB that became unstable after a short time. In region II, for 1.5−7% surfactant and 45−100% SO, stable $C_{12}E_2$ DIBs were obtained. In region III, we observed adhered droplets of the same refractive index (stable DIBs) coexisting with adhered double particles (Janus-like) of different refractive indexes. Increasing the $C_{12}E_2$ concentration in this region increased the number of Janus droplets at the expense of DIBs. The addition of a lipophilic dye, oil blue N, to the oil phase revealed that part of the Janus droplets contained a lipophilic phase (Figure 2b, region III). Finally, region III encompassed another particular region (III′) where pure droplet $C_{12}E_2$ surfactant appeared owing to the reached solubility limit. This state appears at high concentrations of bad solvent and $C_{12}E_{1,2}$, and the surfactant precipitates at the surfaces of the droplets.

Stability of DIBs in Region II of the Phase Diagram. To study the stability of the DIB region and characterize the formed bilayers, we first measured the surface tension of the different interfaces. In the absence of surfactant the interfacial tensions of the aqueous/octane and aqueous/silicone oil are alike: 50 and 47 mN/m, respectively. When $C_{12}E_2$ was added, these values dropped to 9 and 6 mN/m, respectively, whereas for $C_{12}E_1$ both interfacial tensions were around 4 mN/m; the surfactant concentration was kept at 4%.

For each SO content we measured the contact angle between the droplets and determined the adhesion energy. The energy markedly increased with the amount of SO present for $C_{12}E_2$ DIBs and was almost constant for $C_{12}E_1$ DIBs regardless of the SO level (Figure 3). This reveals a fundamental physical difference between these two surfactants to form bilayers due to one PEG motif mismatch on their hydrophilic head. The term $2\gamma_{SS}$ equals $2\gamma_{SL}(\cos\theta)$ and evolves oppositely to the adhesion energy. Higher adhesion conditions, which correspond to lower

DOI: 10.1021/acs.langmuir.5b00749
Langmuir 2015, 31, 6791−6796

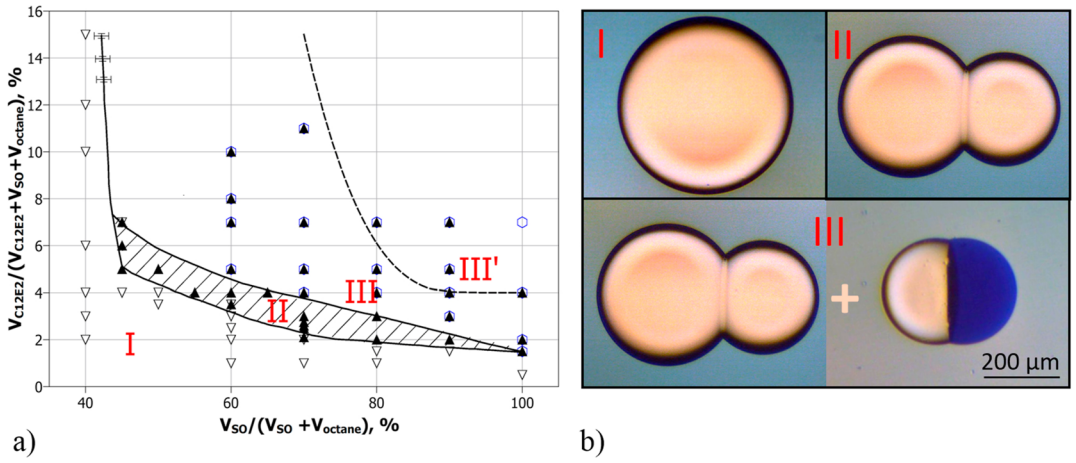

Figure 2. (a) Stability of $C_{12}E_2$ bilayers as a function of silicone oil and octane content. The *x* axis depicts the fraction of silicone oil (SO) in the oil mixture. The *y* axis is the percentage of the surfactant in the total volume of the oil phase. The solid lines delineate the boundaries between the different regions. Maximal error bars are represented. Each data point corresponds to at least three independent experiments. In region I, droplets either coalesce immediately or formed a short-lived DIB disrupted in less than 5 min. In region II, DIBs are stable and lived for more than 5 min. Region III is a two-phase region where stable adhered aqueous droplets forming DIBs coexist with Janus droplets. The latters consist of adhering hydrophilic and lipophilic droplets. Subregion III′ contains droplets of free $C_{12}E_2$ as the surfactant becomes no longer soluble in the oil phase. (b) Snapshots representing the composition of the above-mentioned regions of the $C_{12}E_2$ phase diagram. Transparent phases are water droplets, and blue labels are the lipophilic phase.

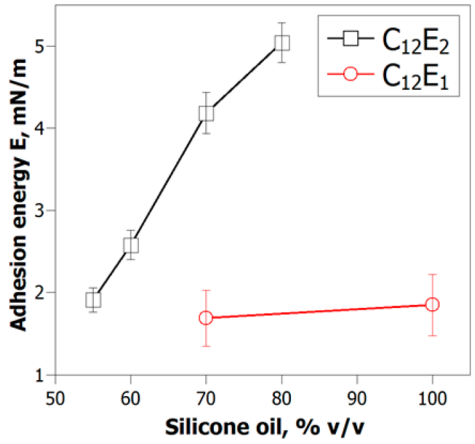

Figure 3. Variation of the adhesion energy against the percentage of silicone oil; each data point corresponds to 15 measurements from 3 independent experiments.

DIB surface tension, better mimic the biological membrane situation and will provide better stability. In that sense, the difference between $C_{12}E_1$ and $C_{12}E_2$ could have a significant effect, for example, on protein recovery or incorporation.

Characterization of Unusual Equilibrium with Janus Particles. The transition to Janus droplets occurred at high surfactant concentrations in region III of the phase diagram. Janus droplets appeared in the microfluidic device very quickly at the droplet formation site. Experimentally, we switched to transparent dishes to be able to directly observe their initiation. In a continuous phase containing 70% SO, 30% octane, and 2.1% $C_{12}E_2$, we added oil blue N as a lipophilic marker. A drop of the aqueous phase was added to the oil solution. We observed the nucleation of a new lipophilic phase (Figure 4), containing a high concentration of the blue lipophilic dye at the water drop surface. This lipophilic phase also seemed to contain water because the apposed water drop decreased in the meantime in size. We repeated the experiment in the presence of rhodamine B labeling the water drop. We indeed observed that the nucleated particles became pink (Figure 5b) by absorbing rhodamine. When visualizing both dyes, this phase was purple (Figure 5c), as it embedded into both dyes. This purple droplet forming the Janus particle was thus made of an amphiphilic surfactant phase.

The thermodynamic equilibrium leads to different morphologies of Janus particles when changing the silicone oil fraction (Figure 6). The contact angle between droplets was around 135° at 70% SO (Figure 6a) and almost 180° at 100% SO in the oil phase (Figure 6b,c). The Janus droplets also appeared in the system with $C_{12}E_1$ surfactant at similar fractions of the surfactant and SO. We were certainly able to visualize them, contrary to $C_{12}E_1$ DIBs formed between aqueous droplets,

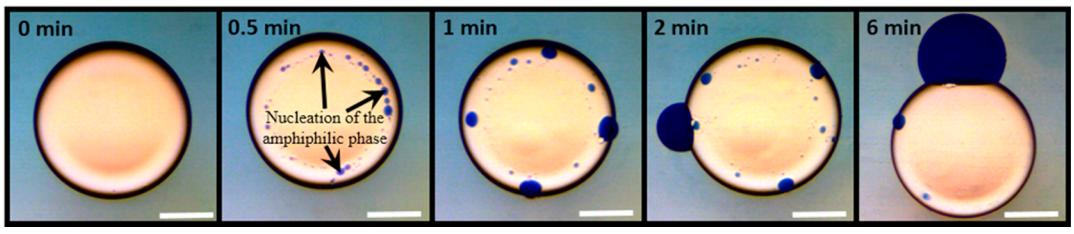

Figure 4. Time sequence showing the formation of a Janus particle. An aqueous drop was immersed in the oil phase containing $C_{12}E_2$ surfactant. Rapid nucleation of the amphiphilic phase happens (colored with oil blue N). After 6 min, a Janus particle is formed. Scale bar: 200 μm.

DOI: 10.1021/acs.langmuir.5b00749
Langmuir 2015, 31, 6791−6796

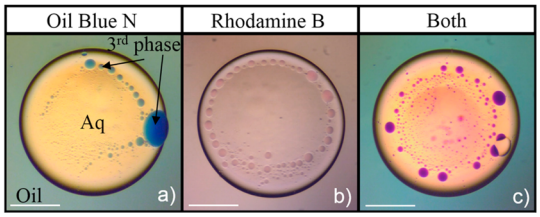

Figure 5. Formation of the amphiphilic phase on a saline drop immersed in oil (70% SO−30% octane). (a) Hydrophobic oil blue N dissolved in the oil is absorbed in the new phase. Likewise, (b) the hydrophilic rhodamine B dye is absorbed. (c) Both dyes are presented in the system and recruited in the amphiphilic phase. Scale bar: 200 μm.

because the aqueous and amphiphilic phases are less prone to fuse.

We observed the Janus droplets under a polarized microscope, and they were not birefringent. We assessed that water molecules absorbed in the amphiphilic phase constituted about 50 ± 6% w/w of that phase (Appendix I). Hence, referring to the $C_{12}E_2$−water phase diagram,[29] the amphiphilic phase was likely a L_3 sponge phase or a mix of L_3 and the inverted cubic V_2 phases. Both phases are isotropic and can be diluted by water and/or oils.[30] This would imply that decreasing temperature would make them transition to a birefringent L_α phase. By cooling the Janus droplets to 10 °C, we observed the expected birefringency of the L_α phase.

At this stage, it is unclear how the system leads to the appearance of Janus droplets instead of simply forming a single amphiphilic phase.

Stability with Longer-Head Surfactants. $C_{12}E_j$ surfactants, $j > 2$, have been used as model bilayers with tunable thickness to study membrane nanoinclusions such as lipids, proteins, and peptides.[14,16,30] Starting with medium-head surfactants, neither $C_{12}E_4$ nor $C_{12}E_5$ formed stable DIBs, and neither merely stabilized emulsions (w/o or o/w) against coalescence. This is probably due to their nearly zero surface curvature because they have respective HLBs of 10.7 and 11.7. These surfactants, however, form stable lamellar phases in aqueous solutions,[13] which basically implied for us that a new formulation would be required to generate DIBs. We succeeded to produce $C_{12}E_4$-$C_{12}E_5$-DIBs using a complex formulation for each surfactant, but for sake of comparison and simplicity, we kept on working with the same SO/octane mixture to study their relative properties.

We worked with a mixture of 70% SO and 30% octane, at high adhesion energy (Figure 3), to induce stable $C_{12}E_2$ DIBs. The total surfactant volume fraction was fixed at 2.1%. We substituted variable amounts of $C_{12}E_2$ surfactant by $C_{12}E_4$ or $C_{12}E_5$, determined by $\varphi = ((V_{C_{12}E_j}(j = 4, 5))/(V_{C_{12}E_j} + V_{C_{12}E_2}))$, and studied the stability of the new DIBs.

For each φ value, we studied about 120 contacts between droplet pairs. We observed that droplets formed either stable DIBs or Janus particles or they fused. For pure $C_{12}E_2$ bilayers ($\varphi = 0$), almost all droplets formed DIBs (91% of total contacts led to stable DIBs). For $\varphi = 2\%$, the percentage of stable DIBs decreased to 70% for $C_{12}E_4$ and to 10% for $C_{12}E_5$ (Figure 7a). This result suggests that, as opposed to $C_{12}E_4$, $C_{12}E_5$ shortens the lifetime of DIBs, by likely provoking the formation of pores in the bilayer and subsequent droplet fusion. Interestingly, as soon as $\varphi \geq 1\%$, Janus droplets appeared (Figure 7b). It is striking that this tiny presence of the longer surfactants significantly shifts the state of the $C_{12}E_2$ in the phase diagram, from the bottom of region II directly to region III (Figure 2). Further titration significantly reduced the DIB stability (Figure 7). No stable DIBs were observed after substitution of $C_{12}E_2$ with 5% $C_{12}E_5$, whereas substitution with 11% $C_{12}E_4$ was required to observe the same inhibition. Larger quantities of $C_{12}E_4$ provoked the formation of a multiple o/w/o emulsion.

Finally, the surfactant mixtures became insoluble in the oil phase once they contained more than $\varphi = 33\%$ of $C_{12}E_5$ or $\varphi = 55\%$ of $C_{12}E_4$.

Observed $C_{12}E_j$ DIB Stability Is Consistent with Predictions. The difference or shift observed between $C_{12}E_4$ and $C_{12}E_5$ in Figure 7 supports the occurrence of pores in C_iE_j lamellar phases reported for these surfactants. Evidence of such defects has been studied both by molecular dynamic simulations[31] and experimentally.[31−33] Whether their occurrence is at room or higher temperature and favored by $C_{12}E_4$ or $C_{12}E_5$ is a matter of controversy.[34,35] Bilayer rupture occurs when pores of a critical size form, leading here to DIB rupture and droplet coalescence. In a simplified model,[36] the free energy of formation, E, of a cylindrical pore with radius r is approximated by $E(r) = 2\pi r\Gamma - \pi r^2\gamma$,[37,38] where γ is the surface tension of the membrane and Γ is the pore line tension. The energy barrier for bilayer rupture is $E_r = \pi\Gamma^2/\gamma$, when a critical

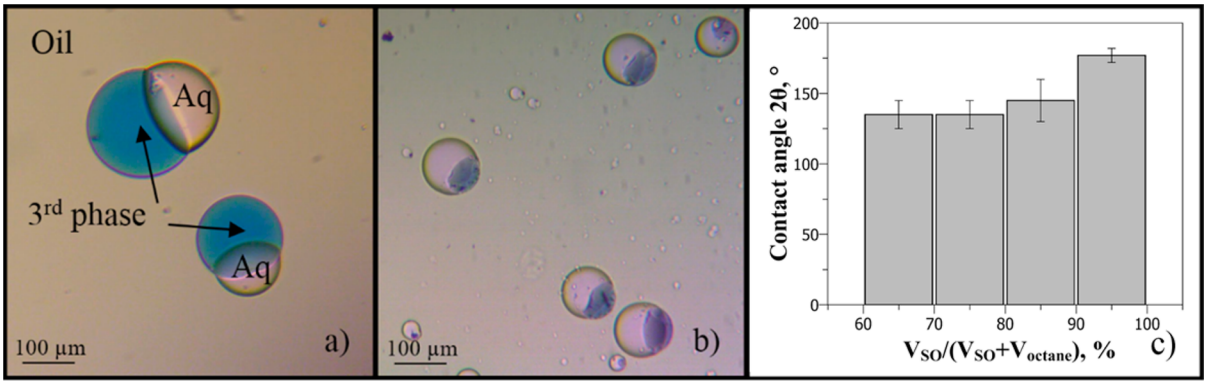

Figure 6. Janus droplets dispersed in oil comprising two spherical portions. One is hydrophilic, and the other absorbs both hydrophilic and lipophilic dyes. Here only oil blue N is present. The topology of the Janus droplets depends on the silicone oil content: (a) for 60−80% v/v SO and (b) for 90−100% SO. (c) The contact angle 2θ for Janus droplets was measured for different volume fractions of silicone oil; a minimum of 15 Janus droplets was studied for each case.

DOI: 10.1021/acs.langmuir.5b00749
Langmuir 2015, 31, 6791−6796

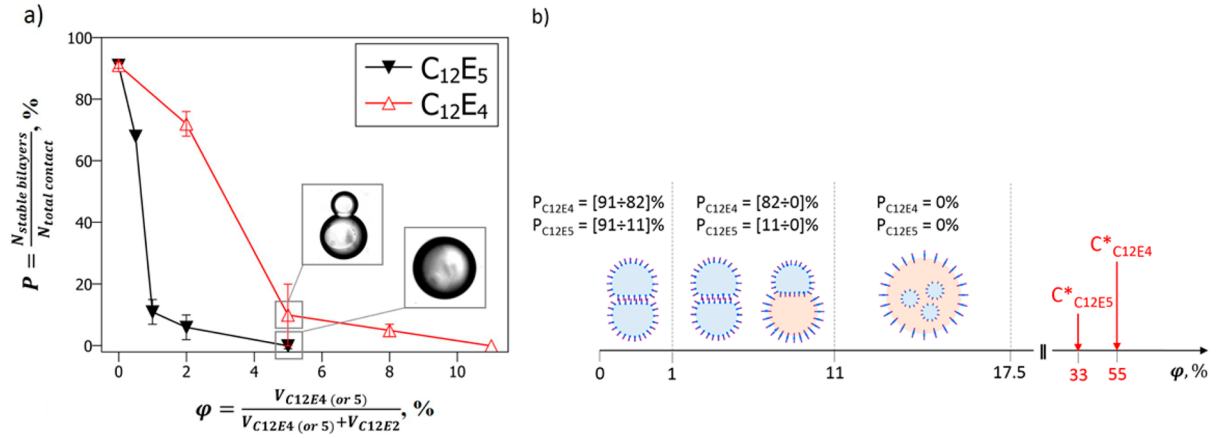

Figure 7. (a) Percentage of stable surfactant bilayers versus φ, the amount of $C_{12}E_{4\ or\ 5}$ in the total surfactant concentration (Δ for $C_{12}E_4$, ▼for $C_{12}E_5$). Each data point corresponds to 100 to 130 measurements. The oil phase is composed of 70% v/v silicone oil and 30% v/v octane. The total surfactant volume fraction is 2.1%. (b) Representation of droplet morphology as a function of φ. Blue is water, and yellow is oil. Arrows depict the solubility limits of the surfactant mixture in the oil phase.

pore radius $R_r = \Gamma/\gamma$ exists in the membrane. From Helfrich's[39] model, $\Gamma = \pi\kappa/h$, where κ is the bending rigidity and h is the thickness of the bilayer. The increase in the head area or decrease in the chain length of the surfactant decreases κ.[40]

Here, when the length of the surfactant polar head was increased from 2 to 4 PEG units and the length of the hydrophobic chain was constant at C_{12}, we measured[41] a slight increase in the membrane thickness (~0.06 nm) and a substantial increase of ~9 Å^2 of the area[41] per polar head. This contributes to reducing the bending modulus from $5.4k_BT$ for $C_{12}E_2$ to $3.2k_BT$ for $C_{12}E_4$. From this variation, the DIB rupture energy $E_r = \pi\Gamma^2/\gamma$ could be expected to be twice lowered from $C_{12}E_2$ to $C_{12}E_4$, which is consistent with our experimental observations (Figure 7). For comparison, most phospholipid bilayers have a higher bending rigidity, around $20k_BT$, and a lower surface tension (<0.1 mN/m) than $C_{12}E_j$; they consequently have a higher rupture energy and a better stability. However, for protein incorporation and folding into membranes, especially for structural studies, having flexible membranes is advantageous, and $C_{12}E_j$ bilayers offer such a possibility.

As opposed to other $C_{12}E_j$ species, $C_{12}E_5$ bilayers exhibit a noticeable interdigitation between the hydrophobic chains of the facing monolayers.[42] This prevented us from determining the $C_{12}E_5$ bending rigidity. Nonetheless, we can expect $\kappa(C_{12}E_4) > \kappa(C_{12}E_5)$[41] for a monolayer because the area per polar head is increased. This is also reflected by their HLBs, which favor better DIB stability with $C_{12}E_4$, as we observed (Figure 7).

To validate the consistency of our studies with the theoretical prediction, we further used surfactants having longer heads, e.g., $C_{12}E_8$ and $C_{12}E_{25}$. They did not allow DIB formation, and their tiny presence in $C_{12}E_2$ DIBs directly led to droplet coalescence. They were more prone to stabilize o/w emulsions, which, with their much higher HLB values, 13.7 and 17.4, respectively, could be expected.

CONCLUSIONS

This work contributes to the ongoing characterization of bilayer properties toward setting optimal conditions for protein/peptide incorporation and recovery and using $C_{12}E_j$,[16] biologically relevant surfactants that maintain the activity of transmembrane proteins. We developed a unique physical chemistry formulation to study the stability of such surfactant bilayers formed by the adhesion of water droplets decorated with a monolayer of the surfactant. Our focus was to study the effect of each surfactant type on pore formation or bilayer/DIB stability. $C_{12}E_2$ mainly formed stable DIBs. We also found unexpected emulsion behaviors that are inherent to the physical aspects of the surfactants. Increased $C_{12}E_{1\ or\ 2}$ surfactant concentration triggered the formation of Janus droplets formed by adhering aqueous and amphiphilic droplets, with the latter consisting of a sponge phase. Knowing the mechanical parameters of $C_{12}E_j$ bilayers has allowed us to interpret the experimental observations well using a simple theoretical framework based on the membrane pore opening energy.

ASSOCIATED CONTENT

Supporting Information

Estimation of the water content in the amphiphilic phase of Janus droplets. The Supporting Information is available free of charge on the ACS Publications website at DOI: 10.1021/acs.langmuir.5b00749.

AUTHOR INFORMATION

Corresponding Author

*E-mail: thiam@lps.ens.fr.

Notes

The authors declare no competing financial interest.

ACKNOWLEDGMENTS

This work was supported in part by ANRs "Assembly" and Investissements d'Avenir no. ANR-10-NANO-06-04.

REFERENCES

(1) Serebryany, E.; Zhu, G. A.; Yan, E. C. Y. Artificial Membrane-like Environments for in Vitro Studies of Purified G-Protein Coupled Receptors. *Biochim. Biophys. Acta* **2012**, *1818*, 225−233.

(2) Khan, M.; Dosoky, N.; Williams, J. Engineering Lipid Bilayer Membranes for Protein Studies. *Int. J. Mol. Sci.* **2013**, *14*, 21561−21597.

(3) Richmond, D. L.; Schmid, E. M.; Martens, S.; Stachowiak, J. C.; Liska, N.; Fletcher, D. A. Forming Giant Vesicles with Controlled Membrane Composition, Asymmetry, and Contents. *Proc. Natl. Acad. Sci. U.S.A.* **2011**, *108*, 9431−9436.

DOI: 10.1021/acs.langmuir.5b00749
Langmuir 2015, 31, 6791−6796

(4) Sackmann, E. Supported Membranes: Scientific and Practical Applications. *Science* **1996**, *271*, 43−48.
(5) Atanasov, V.; Knorr, N.; Duran, R. S.; Ingebrandt, S.; Offenhausser, A.; Knoll, W.; Koper, I. Membrane on a Chip: A Functional Tethered Lipid Bilayer Membrane on Silicon Oxide Surfaces. *Biophys. J.* **2005**, *89*, 1780−1788.
(6) Garavito, R. M.; Picot, D.; Loll, P. J. Strategies for Crystallizing Membrane Proteins. *J. Bioenerg. Biomembr.* **1996**, *28*, 13−27.
(7) Unger, V. M.; Schertler, G. F. Low Resolution Structure of Bovine Rhodopsin Determined by Electron Cryo-Microscopy. *Biophys. J.* **1995**, *68*, 1776−1786.
(8) Rigaud, J.-L.; Chami, M.; Lambert, O.; Levy, D.; Ranck, J.-L. Use of Detergents in Two-Dimensional Crystallization of Membrane Proteins. *Biochim. Biophys. Acta, Biomembr.* **2000**, *1508*, 112−128.
(9) Walian, P.; Cross, T. A.; Jap, B. K. Structural Genomics of Membrane Proteins. *Genome Biol.* **2004**, *5*, 215.
(10) Jiao, J. Polyoxyethylated Nonionic Surfactants and Their Applications in Topical Ocular Drug Delivery. *Adv. Drug Delivery Rev.* **2008**, *60*, 1663−1673.
(11) Cohavi, O.; Corni, S.; De Rienzo, F.; Di Felice, R.; Gottschalk, K. E.; Hoefling, M.; Kokh, D.; Molinari, E.; Schreiber, G.; Vaskevich, A.; et al. Protein−surface Interactions: Challenging Experiments and Computations. *J. Mol. Recognit.* **2010**, *23*, 259−262.
(12) Pasche, S.; Vörös, J.; Griesser, H. J.; Spencer, N. D.; Textor, M. Effects of Ionic Strength and Surface Charge on Protein Adsorption at PEGylated Surfaces. *J. Phys. Chem. B* **2005**, *109*, 17545−17552.
(13) Strey, R.; Schomäcker, R.; Roux, D.; Nallet, F.; Olsson, U. Dilute Lamellar and L3 Phases in the Binary water−C12E5 System. *J. Chem. Soc., Faraday Trans.* **1990**, *86*, 2253−2261.
(14) Gambin, Y.; Lopez-Esparza, R.; Reffay, M.; Sierecki, E.; Gov, N. S.; Genest, M.; Hodges, R. S.; Urbach, W. Lateral Mobility of Proteins in Liquid Membranes Revisited. *Proc. Natl. Acad. Sci. U.S.A.* **2006**, *103*, 2098−2102.
(15) Mitchell, D. J.; Tiddy, G. J. T.; Waring, L.; Bostock, T.; McDonald, M. P. Phase Behaviour of Polyoxyethylene Surfactants with Water. Mesophase Structures and Partial Miscibility (cloud Points). *J. Chem. Soc., Faraday Trans. 1* **1983**, *79*, 975−1000.
(16) Rayan, G.; Adrien, V.; Reffay, M.; Picard, M.; Ducruix, A.; Schmutz, M.; Urbach, W.; Taulier, N. Surfactant Bilayers Maintain Transmembrane Protein Activity. *Biophys. J.* **2014**, *107*, 1129−1135.
(17) Reffay, M.; Gambin, Y.; Benabdelhak, H.; Phan, G.; Taulier, N.; Ducruix, A.; Hodges, R. S.; Urbach, W. Tracking Membrane Protein Association in Model Membranes. *PloS One* **2009**, *4*, e5035.
(18) Brotherus, J. R.; Jacobsen, L.; Jørgensen, P. L. Soluble and Enzymatically Stable ($Na^{++}K^{+}$)-ATPase from Mammalian Kidney Consisting Predominantly of Protomer Aβ-Units: Preparation, Assay and Reconstitution of Active Na^{+}, K^{+} transport. *Biochim. Biophys. Acta, Biomembr.* **1983**, *731*, 290−303.
(19) Lacapere, J. J.; Stokes, D. L.; Olofsson, A.; Rigaud, J. L. Two-Dimensional Crystallization of Ca-ATPase by Detergent Removal. *Biophys. J.* **1998**, *75*, 1319−1329.
(20) Funakoshi, K.; Suzuki, H.; Takeuchi, S. Lipid Bilayer Formation by Contacting Monolayers in a Microfluidic Device for Membrane Protein Analysis. *Anal. Chem.* **2006**, *78*, 8169−8174.
(21) Holden, M. A.; Needham, D.; Bayley, H. Functional Bionetworks from Nanoliter Water Droplets. *J. Am. Chem. Soc.* **2007**, *129*, 8650−8655.
(22) Poulin, P.; Bibette, J. Adhesion of Water Droplets in Organic Solvent. *Langmuir* **1998**, *14*, 6341−6343.
(23) Leptihn, S.; Castell, O. K.; Cronin, B.; Lee, E.-H.; Gross, L. C. M.; Marshall, D. P.; Thompson, J. R.; Holden, M.; Wallace, M. I. Constructing Droplet Interface Bilayers from the Contact of Aqueous Droplets in Oil. *Nat. Protoc.* **2013**, *8*, 1048−1057.
(24) Thiam, A. R.; Bremond, N.; Bibette, J. Adhesive Emulsion Bilayers under an Electric Field: From Unzipping to Fusion. *Phys. Rev. Lett.* **2011**, *107*, 068301.
(25) Thiam, A. R.; Bremond, N.; Bibette, J. From Stability to Permeability of Adhesive Emulsion Bilayers. *Langmuir* **2012**, *28*, 6291−6298.
(26) Yildirim, O. E.; Xu, Q.; Basaran, O. A. Analysis of the Drop Weight Method. *Phys. Fluids* **2005**, *17*, 062107.
(27) Wilkinson, M. C. Extended Use Of, and Comments On, the Drop-Weight (drop-Volume) Technique for the Determination of Surface and Interfacial Tensions. *J. Colloid Interface Sci.* **1972**, *40*, 14−26.
(28) Griffin, W. C. Calculation of HLB Values of Non-Ionic Surfactants. *J. Cosmet. Sci.* **1954**, *5*, 249−256.
(29) Lynch, M. L.; Kochvar, K. A.; Burns, J. L.; Laughlin, R. G. Aqueous-Phase Behavior and Cubic Phase-Containing Emulsions in the $C_{12}E_2$−Water System. *Langmuir* **2000**, *16*, 3537−3542.
(30) Gambin, Y.; Reffay, M.; Sierecki, E.; Homblé, F.; Hodges, R. S.; Gov, N. S.; Taulier, N.; Urbach, W. Variation of the Lateral Mobility of Transmembrane Peptides with Hydrophobic Mismatch. *J. Phys. Chem. B* **2010**, *114*, 3559−3566.
(31) Ferreira, T. M.; Topgaard, D.; Ollila, O. H. S. Molecular Conformation and Bilayer Pores in a Nonionic Surfactant Lamellar Phase Studied with $^{1}H-^{13}C$ Solid-State NMR and Molecular Dynamics Simulations. *Langmuir* **2014**, *30*, 461−469.
(32) Imai, M.; Saeki, A.; Teramoto, T.; Kawaguchi, A.; Nakaya, K.; Kato, T.; Ito, K. Kinetic Pathway of Lamellar → Gyroid Transition: Pretransition and Transient States. *J. Chem. Phys.* **2001**, *115*, 10525−10531.
(33) Medronho, B.; Miguel, M. G.; Olsson, U. Viscoelasticity of a Nonionic Lamellar Phase. *Langmuir* **2007**, *23*, 5270−5274.
(34) Paz, L.; Di Meglio, J. M.; Dvolaitzky, M.; Ober, R.; Taupin, C. Highly Curved Defects in Lyotropic (nonionic) Lamellar Phases. Origin and Role in Hydration Process. *J. Phys. Chem.* **1984**, *88*, 3415−3418.
(35) Constantin, D.; Oswald, P. Diffusion Coefficients in a Lamellar Lyotropic Phase: Evidence for Defects Connecting the Surfactant Structure. *Phys. Rev. Lett.* **2000**, *85*, 4297−4300.
(36) Glaser, R. W.; Leikin, S. L.; Chernomordik, L. V.; Pastushenko, V. F.; Sokirko, A. I. Reversible Electrical Breakdown of Lipid Bilayers: Formation and Evolution of Pores. *Biochim. Biophys. Acta, Biomembr.* **1988**, *940*, 275−287.
(37) Litster, J. D. Stability of Lipid Bilayers and Red Blood Cell Membranes. *Phys. Lett. A* **1975**, *53*, 193−194.
(38) den Otter, W. K. Free Energies of Stable and Metastable Pores in Lipid Membranes under Tension. *J. Chem. Phys.* **2009**, *131*, 205101.
(39) Helfrich, W. Elastic Properties of Lipid Bilayers: Theory and Possible Experiments. *Z. Naturforsch., C.* **1973**, *28*, 693−703.
(40) Würger, A. Bending Elasticity of Surfactant Films: The Role of the Hydrophobic Tails. *Phys. Rev. Lett.* **2000**, *85*, 337−340.
(41) Kurtisovski, E.; Taulier, N.; Ober, R.; Waks, M.; Urbach, W. Molecular Origin of Model Membrane Bending Rigidity. *Phys. Rev. Lett.* **2007**, 98.
(42) Dong, J.; Mao, G. Direct Study of $C_{12}E_5$ Aggregation on Mica by Atomic Force Microscopy Imaging and Force Measurements. *Langmuir* **2000**, *16*, 6641−6647.

DOI: 10.1021/acs.langmuir.5b00749
Langmuir 2015, 31, 6791−6796